Molecular Recognition in Cytochrome P-450: Mechanism for the Control of Uncoupling Reactions†

Paul J. Loida and Stephen G. Sligar*

Departments of Biochemistry and Chemistry and Beckman Institute for Advanced Science and Technology, University of Illinois, Urbana, Illinois 61801

Received June 1, 1993; Revised Manuscript Received August 23, 1993®

ABSTRACT: The pathway for utilization of pyridine nucleotide derived reducing equivalents in the cytochrome P-450 monooxygenase systems has three major branch points. The first is a partitioning between autoxidation of a ferrous, oxygenated heme adduct and input of the second reducing equivalent required for monooxygenase stoichiometry. The second is between dioxygen bond scission and release of two-electron-reduced O_2 as hydrogen peroxide. The third is between substrate hydrogen abstraction initiated by a putative higher valent iron–oxo species and reduction of this intermediate by two additional electrons to produce water in an overall oxidase stoichiometry. For all substrates investigated, the direct release of superoxide at the first branch point never competes with second electron input. In order to elucidate the aspects of molecular recognition of a substrate–P-450 complex which affect these individual branch points in the catalytic cycle, we have measured the NADH-derived reducing equivalents recovered in hydroxylated substrate, hydrogen peroxide, and water for a series of active-site mutants designed to alter the coupling of ethylbenzene hydroxylation. We find that the reaction specificity at the second and third branch points is affected by site-directed mutations that alter the topology of the binding pocket. The increased commitment to catalysis observed for all mutants suggests that active-site hydration is important in the uncoupling to form hydrogen peroxide at the second branch point. The liberation of hydrogen peroxide does not correlate with the location of the mutation in the pocket, as expected if the two-electron-reduced dioxygen-bound intermediate is not directly participating in the substrate activation step. However, a strong correlation is observed between water production at the third branch point and the location and size of the amino acid side chain in the substrate binding site. Larger hydrophobic side chains introduced in the upper regions of the binding pocket increase the ratio of hydroxylated product to water production by 2–4-fold relative to wild-type, while similar substitutions in residues near the heme plane result in diminished product. Overall, the partitioning between hydroxylation and oxidase activities varies by over 65% due to the location of nonpolar substituents engineered into the active site. Substrate access to the heme is the key factor for tight coupling at the level of the putative iron–oxo species. These results are further evidence that a discrete intermediate containing a single oxygen atom (e.g., a ferryl–oxo complex, $[FeO]^{3+}$) is the precursor to both substrate hydroxylation and the input of two additional electron equivalents to form water.

The heme-containing mixed-function monooxygenases referred to as cytochrome P-450 are ubiquitous in biological systems and play important roles in the synthesis of steroids and fatty acids and the metabolism of xenobiotics. This class of enzymes catalyzes a wide variety of chemical transformations including hydroxylation, epoxidation, dealkylations, carbon–carbon bond scission, and reductive dehalogenation (Guengerich, 1991). While the substrate specificity differs between individual isozymes, the selectivity of the superfamily as a whole is quite broad, ranging from molecules as small as ethane to peptides and large polycyclic hydrocarbons. Cytochrome $P\text{-}450_{cam}$, isolated from the soil bacterium *Pseudomonas putida*, catalyzes the 5-*exo*-hydroxylation of camphor as the first step in a metabolic pathway that enables the organism to be sustained with camphor as its sole source of carbon (Sligar & Murray, 1986). It is the terminal member of a three-protein electron-transfer chain in which the reducing equivalents originating in nicotinamide adenine dinucleotide, reduced form (NADH),[1] are shuttled through an FAD-containing flavoprotein, putidaredoxin reductase, and a 2Fe–2S ferredoxin, putidaredoxin. In addition to its high stereospecificity and regiospecificity, the reaction with camphor is catalyzed with absolute efficiency with respect to the coupling of NADH to hydroxylated product (Gelb *et al.*, 1982; Gould *et al.*, 1981). The coupling is decreased for the epoxidation of dehydrocamphor (Gelb et al., 1982b) and in the presence of substrate analogs and small carbon compounds that are structurally dissimilar to camphor (Atkins & Sligar, 1989; Fruetel *et al.*, 1992; Loida & Sligar, 1993). The electron equivalents that are not utilized to oxidize substrate are liberated from intermediate steps of the P-450 reaction cycle in the form of superoxide, hydrogen peroxide, or water as illustrated in Figure 1 (Atkins & Sligar, 1987; Gorsky *et al.*, 1984).

In cytochrome $P\text{-}450_{cam}$, atmospheric dioxygen binds to the substrate-bound ferrous form of the enzyme to generate the last observable intermediate of the reaction cycle (Es-

† This work was supported by National Institutes of Health Grants GM33775 and GM33776.

* To whom correspondence should be addressed at the Department of Biochemistry, University of Illinois at Urbana–Champaign.

® Abstract published in *Advance ACS Abstracts,* October 1, 1993.

[1] Abbreviations: F87, phenylalanine-87 of cytochrome $P\text{-}450_{cam}$; Y96, tyrosine-96; T101, threonine-101; T185, threonine-185; L244, leucine-244; V247, valine-247; G248, glycine-248; V295, valine-295; D297, aspartate-297; I395, isoleucine-395; V396, valine-396; T101M, single mutant generated by replacing wild-type threonine-101 with methionine; this notation applies to T101I, T185V, T185L, T185F, V247A, V247M, and V295I, and also T101M–T185F–V247M which is a triple mutant with the respective substitutions; NADH, nicotinamide adenine dinucleotide in the reduced form; R–OH, hydroxylated ethylbenzene.

0006-2960/93/0432-11530$04.00/0

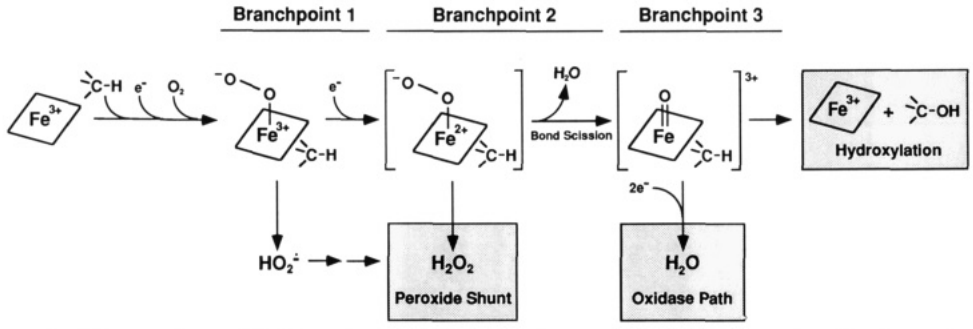

FIGURE 1: Schematic of the cytochrome P-450 reaction cycle illustrates the unproductive pathways that give rise to the side products hydrogen peroxide and water. The one-electron-reduced oxy-P-450 intermediate marks the first branch point at which autoxidation or second-electron reduction occurs. The two-electron-reduced peroxy-P-450 species undergoes either dioxygen bond cleavage or peroxide release at the second branch point. At the third fork, the putative iron–oxo intermediate is partitioned between substrate hydroxylation and additional reduction via the oxidase pathway to form water.

tabrook *et al.*, 1971; Ishimura *et al.*, 1971; Tyson *et al.*, 1972). As in the case of the oxygen transport proteins, this oxy complex disproportionates to yield ferric hemoprotein and superoxide anion (Sligar *et al.*, 1974). Site-directed mutagenesis experiments suggest that a hydrogen bond formed between a highly conserved threonine residue in the P-450$_{cam}$ active site and the distal oxygen atom of the complex stabilizes the oxy–ferrous intermediate prior to dioxygen bond scission (Imai *et al.*, 1989; Martinis *et al.*, 1989). The presence of a small molecule bound in the active site of P-450$_{cam}$ increases the lifetime of this species by 100-fold (Lipscomb *et al.*, 1976).

The rate of autoxidation, measured by the breakdown of the isolated oxy-P-450$_{cam}$ intermediate, does not always account for the hydrogen peroxide produced under steady-state turnover conditions (Martinis *et al.*, 1989). It is likely that a two-electron-reduced oxygen-bound transient is formed after the second electron transfer and is responsible for the majority of the hydrogen peroxide liberated. While the enzyme will accept molecules of widely varied structure, the peroxide recovered in some cases accounts for greater than 98% of the total NADH utilized (Fruetel *et al.*, 1992). Studies with the reconstituted P-450$_{cam}$ system have shown that uncoupling to peroxide is suppressed when the substrate is structurally complementary to the enzyme active site (Atkins & Sligar, 1989).

A third mode of uncoupling (Figure 1) in cytochrome P-450 is the four-electron reduction of dioxygen to water and results in a stoichiometry of 2:1 for the consumption of NADH and molecular oxygen (Staudt *et al.*, 1974). The degree of this oxidase activity is not dependent on the concentration of free hydrogen peroxide in solution and can be stimulated by the fluorinated and deuterated analogs of viable substrate molecules (Atkins & Sligar, 1987; Dawson, 1993, personal communication). As in the case of hydrogen peroxide, water production varies widely with different substrates and is inhibited in P-450$_{cam}$ when the bound molecule is tightly packed into the active site (Atkins & Sligar, 1989; Gorsky *et al.*, 1984). There is strong evidence that the mechanism of input for the extra two electrons in the oxidase pathway is at the level of a single oxygen-bound iron complex (Atkins & Sligar, 1987, 1988a; Zhukov & Archachov, 1982) and that a putative iron–oxo species marks a distinct branch point after dioxygen bond scission at which substrate oxidation or additional reduction to form water can occur.

While the pathways in the reaction cycle that give rise to these various reduced oxygen side products are established, the determinants for the level of uncoupling to hydrogen peroxide and water are not understood. Deuterium isotope studies with norcamphor indicate that smaller substrates sample multiple orientations in the active site within the lifetime of the iron–oxo species and that the facility for oxidation of a substrate carbon atom is strongly related to its proximity to the hydroxylating intermediate (Atkins & Sligar, 1987). Theoretical investigations of substrate orientation and mobility are consistent with this interpretation, and molecular dynamics simulations suggest that substrate motions occur on the subnanosecond time scale (Bass *et al.*, 1992b; Collins & Loew, 1988; Filipovic *et al.*, 1992; Paulsen *et al.*, 1991). Equilibrium and kinetic analysis of the ferric spin-state equilibrium for a range of camphor analogs demonstrates that water access to the heme iron is dependent upon the structure of the particular molecule that is bound in the active site (Fisher & Sligar, 1987; Raag & Poulos, 1989). Non-native substrates appear to be more mobile in the active site and fail to displace sequestered solvent from the buried heme pocket. On the basis of these observations, there are two plausible explanations for the observed oxidase activity: (1) the residence time of the substrate near the oxidizing species is variable such that electron transfer to reduce the ferryl intermediate competes with substrate hydroxylation; and (2) residual water in the active site serves as a proton donor, aiding the breakdown of the iron–oxo species in the presence of the native redox-transfer chain. The hydration of the active site may also be important in the uncoupling of oxy- and peroxy-P-450 intermediates to form hydrogen peroxide.

In previous work, we have reported a series of P-450$_{cam}$ mutants which altered the coupling of reducing equivalents to product in the hydroxylation of ethylbenzene, although the individual contributions from the peroxide and water release branch points were not distinguished (Loida & Sligar, 1993). In this paper, we (1) document how the levels of peroxide and water produced in the metabolism of ethylbenzene are altered by directed amino acid substitutions that introduce larger aliphatic side chains at defined positions around the perimeter of the active site, (2) determine whether the changes in peroxide and water production are correlated with the location and volume of the added steric bulk in the active site and define a relationship between substrate oxidation, water formation, and peroxide production, (3) elucidate the role of the active-site mutants in substrate positioning and water access and its relationship to peroxide and water generation, and (4) propose a molecular mechanism for the control of the peroxide and oxidase branch points in the cytochrome P-450 reaction.

MATERIALS AND METHODS

Reconstituted Enzyme System. Wild-type P-450$_{cam}$, P-450$_{cam}$ mutants, putidaredoxin, and putidaredoxin reductase were expressed and purified according to standard procedures

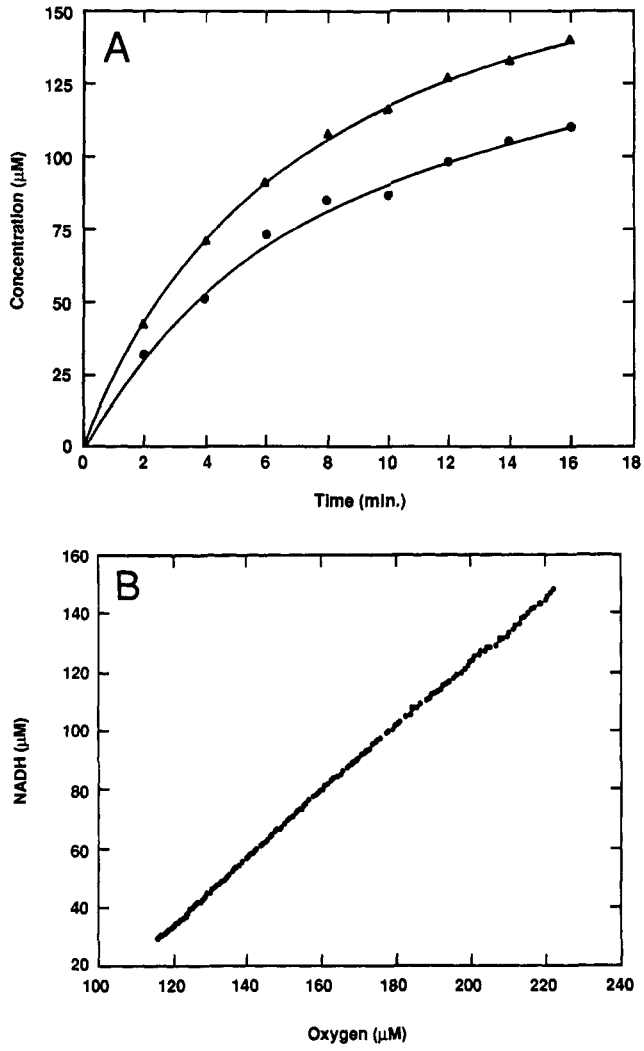

FIGURE 2: (A) Hydrogen peroxide formation relative to NADH consumption. The liberation of hydrogen peroxide in the presence of ethylbenzene was determined along with NADH oxidation as described under Materials and Methods. NADH is denoted by triangles, and hydrogen peroxide is shown in circles. (B) NADH oxidation and oxygen consumption were determined simultaneously by monitoring the reaction spectrophotometrically at 340 nm and potentiometrically with a Clark electrode (Materials and Methods).

(Davies *et al.*, 1990; Gunsalus & Wagner, 1978; Martinis, 1990). All other materials were prepared as previously reported (Loida & Sligar, 1993). The concentrations of the components of the reconstituted enzyme system used in the hydrogen peroxide assays and oxygen determinations were typically 0.5 μM P-450$_{cam}$, 5 μM putidaredoxin, 1 μM putidaredoxin reductase, 50 mM Tris-HCl, pH 7.0, 50 mM KCl, and 500 μM substrate.

Hydrogen Peroxide Production. The hydrogen peroxide produced in the reaction with ethylbenzene was quantitated using an iron thiocyanate colorimetric assay as previously described (Atkins & Sligar, 1987; Fruetel *et al.*, 1992), and the oxidation of NADH was monitored at 340 nm using an extinction coefficient of 6.22 mM^{-1} cm^{-1}. The reaction was initiated by making the solution 250 μM in NADH; at 2-min intervals, an appropriate volume of the reaction mixture was removed and quenched with acid as the first step in the peroxide assay (Figure 2A). The reaction was sampled 8 times and the entire procedure repeated. The ratio of hydrogen peroxide produced to NADH utilized was calculated and is reported in Table I.

Oxygen Consumption. Oxygen and NADH consumptions were measured simultaneously by utilizing a reaction cell fitted with a Clark electrode (Gerber & Sligar, 1992). NADH oxidation was monitored by optical absorption using an extinction coefficient of 6.22 mM^{-1} cm^{-1} at 340 nm. The reaction was initiated with 150 nmol of NADH at 20 °C. The output from the spectrophotometer and oxygen electrode was transferred to a 25-MHz Gateway 2000 PC every 0.5 s and converted to concentrations of NADH and oxygen using the data acquisition software Lab Windows 2.0. At least three determinations were made for each protein–substrate combination. The concentration of NADH was plotted versus the concentration of oxygen, and the slope of the line was determined (Figure 2B). The correlation coefficient obtained by this fitting procedure was always greater than 0.95. The initial concentration of oxygen was greater than the initial concentration of NADH such that the intercept in Figure 2B corresponds to 80–90 μM excess oxygen remaining in the solution after the complete oxidation of NADH. In experiments for which the NADH was completely utilized, the concentration of oxygen reached a minimum value and remained constant. There was no further uptake of oxygen after the NADH was depleted. The oxygen consumed is reported in Table I as a percentage of the NADH utilized. Control experiments with camphor as the substrate resulted in an average slope of 1.02.

Ferric Spin-State Equilibrium and Dissociation Constant. The equilibrium dissociation constants (K_D) were determined by monitoring the differences in the optical absorbance spectrum of substrate-free and -bound cytochrome P-450$_{cam}$. Because of the effect of ethanol on the ferric spin-state equilibrium and the small changes in the high-spin population observed with several of the mutants, independent additions of the substrate to the protein were made instead of cumulative additions as in a typical titration. Five-hundred-microliter aliquots of 10 μM substrate-free protein (50 mM Tris, 50 mM KCl) were added to 500 μL of camphor or ethylbenzene dissolved in water (from ethanol stock) to achieve the desired substrate concentration. The optical absorbances at 417 nm and the isosbestic point at 404 nm were used to calculate the high-spin fraction of the enzyme as previously reported (Hui Bon Hoa & Marden, 1982), and the changes in this parameter were used to determine K_D (Table II) (Weber, 1973).

The ferric spin equilibrium of P-450$_{cam}$ is driven toward the high-spin form under saturating substrate concentrations. It is dependent on the particular small molecule bound and is often altered by active-site mutations (Atkins & Sligar, 1988b; Fisher & Sligar, 1985). The maximum change in the spin-state equilibrium upon camphor and ethylbenzene binding to P-450$_{cam}$ was calculated, and the results are reported as the percent high spin fraction of the protein in Table II.

RESULTS

In the cytochrome P-450$_{cam}$ mutants described herein, large hydrophobic side chains (leucine, isoleucine, methionine, and phenylalanine) are substituted for the small nonpolar residue valine or the small polar residue threonine. The mutations are distributed over the surface of the active site with two located near the plane of the heme, T101 and V295, and two that are positioned a longer distance from the heme group in the upper region of the binding pocket, V247 and T185 (Figure 3A). On the basis of the Vornoi volume of the amino acid side chains and the molecular volume of camphor, the single substitutions decrease the open volume of the P-450$_{cam}$ active site by 10–25%, and the triple mutant closes the binding pocket to half its original size (Raag & Poulos, 1991; Richards, 1977).

Table I: Effect of Active-Site Mutations on Product Formation, Reactant Consumption and Branching Ratios of Uncoupling

P-450$_{cam}$	1-phenylethanol[a]	oxygen[a]	water via oxidase path[a,b]	hydrogen peroxide[a]	NADH oxidation rate[c]
wild-type	5.0 ± 0.5	89 ± 4	11 ± 4	77 ± 4	52 ± 4
single mutants					
T101M	0.1 ± 0.05	76 ± 6	24 ± 6	61 ± 5	14 ± 2
T101I	2.2 ± 0.1	90 ± 4	10 ± 4	83 ± 5	26 ± 3
T185V	5.0 ± 0.5	87 ± 5	13 ± 5	76 ± 4	49 ± 3
T185L	13 ± 1	88 ± 4	12 ± 4	72 ± 3	64 ± 4
T185F	13 ± 1	93 ± 3	7 ± 3	76 ± 4	11 ± 1
V247A	3.0 ± 0.4	52 ± 5	48 ± 5	4 ± 3	30 ± 3
V247M	12 ± 1	87 ± 4	13 ± 4	67 ± 3	40 ± 4
V295I	0.3 ± 0.1	83 ± 4	17 ± 4	68 ± 4	41 ± 2
triple mutant					
T101M–T185F–V247M	13 ± 1	80 ± 6	20 ± 6	52 ± 5	23 ± 2

[a] Expressed as a percentage of the NADH equivalents oxidized. [b] Method of calculation from oxygen consumption is outlined under Results. [c] Nanomoles of NADH per minute per nanomoles of P-450. Taken from the data collected for peroxide production and oxygen consumption.

Table II: Substrate Binding Parameters for Active-Site Mutants

	camphor		ethylbenzene	
P-450$_{cam}$	% HS[a]	K_D (μM)	% HS[a]	K_D (μM)
wild-type	91	1.4 ± 0.3	33	90 ± 15
single mutants				
T101M	67	34 ± 4	5	70 ± 18
T185L	62	0.8 ± 0.2	24	44 ± 6
T185F	24	13 ± 2	4	80 ± 20
V247A	95	2.9 ± 0.6	35	60 ± 11
V247M	74	3.3 ± 0.7	31	81 ± 13
V295I	95	1.7 ± 0.3	25	75 ± 10
triple mutant				
T101M–T185F–V247M	40	49 ± 7	5	52 ± 10

[a] The ferric spin-state equilibrium is expressed as the percentage of high-spin form under saturating substrate concentrations.

Autoxidation and Oxidase Activities. Wild-type P-450$_{cam}$ hydroxylates ethylbenzene to give one regioisomer, 1-phenylethanol, with 5% of the reducing equivalents coupled to product formation (Loida & Sligar, 1993). Of the NADH oxidized in the reaction, 77% is used to produce hydrogen peroxide, leaving 18% of the reducing equivalents still unaccounted for, presumably utilized to form water via the oxidase pathway (Table I). The four-electron reduction of oxygen to water is quantified by measuring the ratio of NADH and oxygen consumed in the reaction. The value of 1.12 for wild-type P-450$_{cam}$ indicates that 22% of the reducing equivalents are shunted into the oxidase pathway.

$$\frac{\text{NADH}}{\text{O}_2} = \frac{100 \text{ equiv NADH}}{X \text{ equiv O}_2}$$

$$100 \text{ equiv NADH} - X \text{ equiv O}_2 = Y \text{ equiv H}_2\text{O produced via the oxidase pathway}$$

$$Y \text{ equiv H}_2\text{O (oxidase)} \times \frac{2 \text{ equiv NADH}}{\text{H}_2\text{O (oxidase)}} = \% \text{ NADH (oxidase)}$$

The results obtained from two independent methods for measuring the oxidase activity are in agreement within experimental error: (1) substrate oxidation and hydrogen peroxide production; (2) oxygen and NADH consumption. Likewise, measurements of the hydrogen peroxide and 1-phenylethanol formed and the dioxygen utilized are internally consistent for all mutants, and these data are further evidence that cytochrome P-450$_{cam}$ produces water when catalyzing the hydroxylation of uncoupled substrates.

The relative amounts of 1-phenylethanol, peroxide, and water produced in the reaction are significantly changed by many of the active-site mutations (Table I). The 1-phenylethanol ranges from 0.1% with T101M to 13% with T185L.

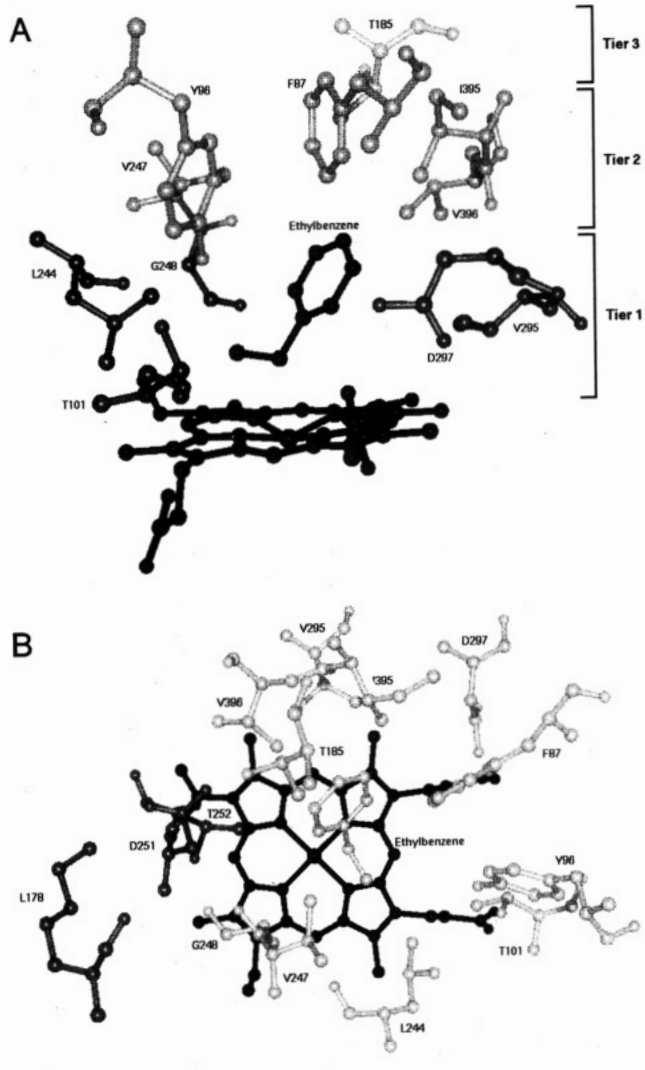

FIGURE 3: (A) "Side-on" view of the cytochrome P-450$_{cam}$ active site with a model of ethylbenzene oriented for benzylic hydroxylation. Residues in Tier 1, shown in dark gray, are positioned near the heme and include T101, L244, V295, G248, and D297. Tiers 2 and 3, shaded light gray, form the upper region of the binding pocket and are comprised of residues F87, Y96, T185, V247, I395, and V396. The heme and ethylbenzene are black. (B) The top-down view includes residues of the putative charge relay: K178, D251, and T252. The proton-transfer pathway, shown in dark gray, is positioned over pyrrole ring A, while the substrate and the side chains lining the active site, shaded light gray, are above rings A, B, C, and D.

Water production is as low as 7% for T185F and as high as 20% for T101M–T185F–V247M and 95% for V247A. The liberation of hydrogen peroxide varies from 4% with V247A

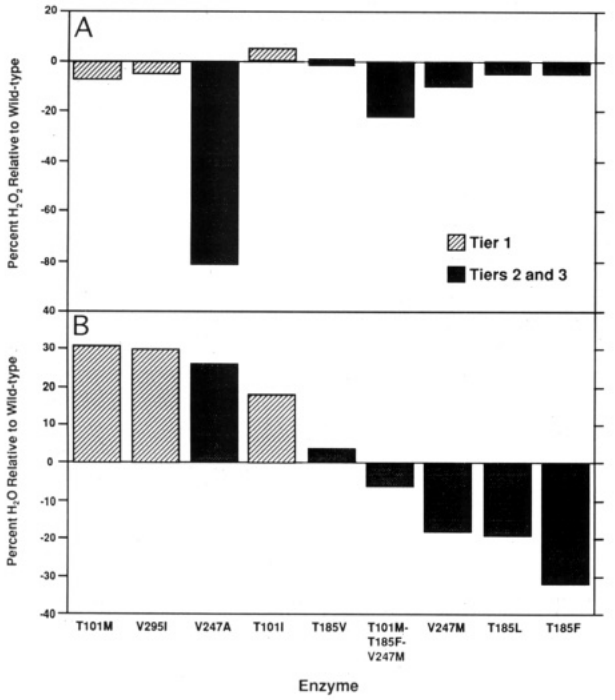

FIGURE 4: Reaction specificity differences between wild-type cytochrome P-450$_{cam}$ and a series of active-site mutants in the hydroxylation of ethylbenzene. The large hydrophobic side chains of Ile, Leu, Met, and Phe were substituted for Val and Thr at four positions in the binding pocket. Residues in Tier 1 are located near the heme and are shown by hatched bars, and residues in tiers 2 and 3 are distant from the heme and are indicated by solid bars. (A) Each bar represents the difference in the partitioning of oxygen to peroxide at the second branch point for the mutants minus wild-type P-450$_{cam}$. Hydrogen peroxide is expressed as a percentage of the total oxygen consumed in the reaction. (B) Each bar represents the difference in water formed at the oxidase pathway relative to wild-type P-450$_{cam}$. Water is expressed as a percentage of the total oxygen equivalents passing through the third reaction branch point. For active-site residues in Tiers 2 and 3, there is a negative correlation between the side-chain packing volume and the production of water. This relationship is reversed for mutations in Tier 1.

and 52% with T101M–T185F–V247M to 83% with T101I. The roughly isosteric substitution T185V results in very small changes in the reaction specificity at both the second and third branch points.

An illustration of the branch points in the P-450 reaction is presented in Figure 1. The oxy-P-450 intermediate autoxidizes at a slow rate relative to the steady-state cycling of the system; therefore, at the first branch point, uncoupling to form superoxide does not compete with second-electron reduction. The peroxy-P-450 species marks the second branch point at which dioxygen bond scission or hydrogen peroxide release can occur. At the third fork, substrate oxidation competes with the oxidase pathway to determine the fate of the iron–oxo species. The data were analyzed further by determining the partitioning of reaction intermediates at branch points 2 and 3 and searching for potential correlations with the location, size, and shape of the amino acid substitutions introduced in the active site.

The reducing equivalents used in the reduction of the putative $[FeO]^{3+}$ intermediate to water enter the reaction cycle at the third branch point. This effect is accounted for in the analysis of branch point 2 by dividing the hydrogen peroxide produced by the total dioxygen used, not the total NADH consumed. Nearly all of the active-site mutants lower the flux through the peroxide shunt, but the magnitude of the change is not related to the position of the substitution (Figure 4A). With the exception of V247A and T101M–T185F–V247M, most of the mutant cluster within about −10% of the value for wild-type P-450$_{cam}$. The fact that the triple mutant causes a substantial decrease in hydrogen peroxide production relative to the single mutants indicates that active-site polarity and hydration are important to the stability of the oxy-P-450$_{cam}$ intermediates. With V247A, dioxygen bond scission accounts for greater than 90% of the O_2 equivalents at the second reaction branch point, suggesting that this mutation has a secondary effect on the reaction by altering the oxygen activation chemistry.

In the quantitation of branch point 3, the reducing equivalents lost to hydrogen peroxide are ignored. By dividing the quantity of water formed by the total non-autoxidative products, the analysis accurately reflects the partitioning of reducing equivalents between hydroxylation of substrate and reduction to water at the level of the $[FeO]^{3+}$ species. In Figure 4B, the percentage of water generated relative to wild-type is plotted for the set of mutations. This treatment reveals a strong relationship between the oxidase activity and the position and size of the active-site substitution. For active-site residues relatively distant from the heme, there is a negative correlation between side-chain packing volume and the production of water. Compared to wild-type, V247A lowers the ratio of R–OH/H_2O from 0.51 to 0.08, while T185L and V247M increase the fraction of 1-phenylethanol to about 1.0. When the larger and rigid amino acid phenylalanine is substituted at T185, the oxidation of substrate is increased even further, and alcohol is the major product (R–OH/H_2O = 1.9). A very small change is observed with the essentially isosteric mutant T185V. The relationship between side-chain volume and oxidase branch point is reversed for mutations in tier 1 of the active site. T101I decreases the ratio of R–OH/H_2O production to 0.20, and with T101M and V295I, essentially all of the oxidizing intermediate is reduced to water with R–OH/H_2O ratios of 0.004 and 0.02, respectively. The triple mutant T101M–T185F–V247M results in a small increase in the recovery of the alcohol with the opposing trends for T101M versus T185F and V247M dominated by the latter two residues. The influence of the mutations on 1-phenylethanol production is more dramatic after correcting for the NADH lost in hydrogen peroxide. The overall coupling to hydroxylated product varies 13%, but the partitioning with water at the third reaction branch point ranges over 65%.

Dissociation Constants and Ferric Spin State. The dissociation constants and equilibrium spin conversions for ethylbenzene and camphor binding to the active-site mutants are summarized in Table II. There is no correlation between either of these measured parameters and the distance of the mutated residue from the heme plane (see Figure 3A) or the formation of 1-phenylethanol, peroxide, and water in the reaction with ethylbenzene. Most of the mutants bind ethylbenzene more tightly and camphor less tightly relative to the wild-type protein. This is consistent with a smaller binding cleft produced when extra steric bulk is added to the active site in the form of leucine, isoleucine, methionine, and phenylalanine side-chain substitutions. One exception is the T185L mutant which associates with camphor more readily than the wild-type P-450$_{cam}$, and V247A which binds ethylbenzene tighter than wild-type.

DISCUSSION

In the resting state of cytochrome P-450$_{cam}$, the ferric low-spin iron is six-coordinate aquo-liganded and adjacent to five additional molecules of water that are sequestered in the active site (Poulos *et al.*, 1987). The substrate-dependent change

in the ferric spin equilibrium favors the high-spin form of the enzyme and is correlated with the on-rate of water to the iron, the energy of activation for the first electron transfer, and a 130-mV increase in the redox potential of the iron which results in a favorable thermodynamic driving force for the reduction of P-450$_{cam}$ by putidaredoxin (Fisher & Sligar, 1985; Sligar, 1976; Sligar & Gunsalus, 1976). If the small molecule bound is not structurally complementary to the active site, water retains partial access to the iron, the conversion to the high-spin form is incomplete, and the influx of reducing equivalents necessary for maximum cycling of the enzyme is not realized. After oxygen binds to ferrous substrate-bound P-450$_{cam}$ and the second electron is transferred, a peroxy–heme complex is believed to undergo dioxygen bond scission to form the putative oxo–ferryl species which abstracts a substrate hydrogen and via the oxygen-rebound mechanism returns ·OH to the substrate radical, regenerating the ferric resting state of the heme protein (Groves & McCluskey, 1976). Both hydrogen abstraction and subsequent radical addition steps are stereochemically controlled (Gelb *et al.*, 1982). In cytochrome P-450$_{cam}$, the absolute regiospecificity and sterospecificity of hydroxylation and the high reaction efficiency are a consequence of specific substrate–protein contacts which serve to constrain camphor in the binding pocket and position the 5-carbon adjacent to the iron.

The X-ray structure of cytochrome P-450$_{cam}$ reveals that the active site is a buried cleft largely isolated from solvent with 12 amino acid residues from 6 different segments of secondary structure along with the protoporphyrin IX forming the inside surface of the pocket (Poulos *et al.*, 1987). There is a single hydrogen bond formed between Y96 and the ketone of camphor that plays a role in substrate binding, positioning the substrate in the active site, and preserving the ferric spin-state equilibrium of the hemoprotein (Atkins & Sligar, 1988b; DiPrimo *et al.*, 1990; White *et al.*, 1984). Extensive hydrophobic contacts are made with camphor as the shape of the active site is highly complementary to the three-dimensional structure of this molecule. Site-directed mutagenesis experiments have shown that F87, T101, T185, V247, and V295 all contribute to the orientation of substrates in the active site through hydrophobic interactions (Atkins & Sligar, 1989; Bass *et al.*, 1992; Loida & Sligar, 1993).

As shown in Figure 3A,B, the side chains of residues T101 and V295 are located on opposite sides of pyrrole ring D and are positioned near to the iron in a plane that is parallel to the heme and just above the prosthetic group. For discussion, this layer of residues is referred to as Tier 1 and also includes L244, G248, T252, and D297. Residue V247 is positioned up and away from the heme over pyrrole rings B and C and defines a second layer of residues. Tier 2 is made up of F87, Y96, V247, I395, and V396 and is parallel to and above Tier 1. T185 essentially forms a cap above Tiers 1 and 2, and we consider this to be the only residue in Tier 3 (Figure 3A).

Previously, we have reported site-directed mutants of cytochrome P-450$_{cam}$ that alter the *overall* coupling of ethylbenzene hydroxylation (Loida & Sligar, 1993). Larger hydroprobic side chains introduced in Tiers 2 and 3 were found to nearly triple substrate hydroxylation relative to wild-type, while similar substitutions in residues near the heme diminished 1-phenylethanol production. In this paper, we have determined the fate of the uncoupled reducing equivalents and examined the relationship between the active-site mutations and the individual reaction cycle branch points.

In the cytochrome P-450 reaction, there are three shunt pathways by which NADH-derived reducing equivalents are utilized to make products other than oxidized substrate (Figure 1). At the first branch point, the oxy-P-450 intermediate either autoxidizes or undergoes second-electron reduction. The rate of autoxidation is slow, such that under steady-state reaction conditions the liberation of superoxide does not usually contribute to the uncoupling of the system. At the second branch point, the peroxy-P-450 intermediate either disproportionates to hydrogen peroxide and ferric cytochrome or proceeds along the native reaction coordinate and undergoes oxygen bond cleavage to form the putative iron–oxo species. The third branch point is the oxidase pathway whereby $[FeO]^{3+}$ can undergo two additional electron reduction to form water or commit to hydroxylation by abstracting a substrate hydrogen atom. If the hydroxylation and oxidase activities share a common branch point distinct from the peroxy-P-450 intermediate and the peroxide shunt, then one would expect the recovery of water to be highly correlated with the position of the amino acid substitution and the hydrogen peroxide production to be independent of the mutation. When the reducing equivalents lost in peroxide are accounted for in the analysis of the water production, a striking relationship between the oxidase activity and the site of the mutated side chain is revealed. The 1-phenylethanol production and four-electron reduction to water vary inversely as a function of the position and size of the amino acid substitution (Figure 4B). These results are consistent with, and offer additional evidence for, a discrete intermediate subsequent to dioxygen bond scission from which oxygen atom insertion into a carbon–hydrogen bond or two additional electron reduction to form water can occur. Peroxide liberation is not correlated to ethylbenzene orientation in the active site as expected if the one- and two-electron-reduced dioxygen-bound species are not active in substrate oxidation (Figure 4A).

The reaction specificity of cytochrome P-450 is controlled by the topological features of the binding pocket. The switch in reaction chemistry from hydroxylation to oxidase activity upon engineering steric bulk around the perimeter of the active site causes the ratio of hydroxylated substrate to water production to change by over 400-fold, and is strong evidence that substrate positioning is the key factor for tight coupling at the level of the putative iron–oxo species. Adding large nonpolar groups in Tier 1 reduces the hydroxylation of ethylbenzene by "pushing" the substrate away from the heme (Figure 3A). Under these conditions, perhaps the longer lifetime of the $[FeO]^{3+}$ allows for more facile input of two additional electrons from the redox partner protein putidaredoxin and subsequent release of water. Extended side chains are more conducive to uncoupling than β-branched amino acids as shown by the additional increase in water production in going from the isoleucine to methionine substitution at residue T101. Moving the methyl group from the β-carbon to the δ-carbon and adding the larger sulfur atom allow the T101M side chain to extend over the heme and effectively block the approach of ethylbenzene to the iron. With T101M and V295I, the hydroxylation of ethylbenzene by P-450$_{cam}$ is essentially eliminated. Substituting larger residues at positions in the pocket that are distant from the heme "pushes" the substrate toward the oxidizing intermediate. The greater residence time of the ethylbenzene benzylic carbon at the $[FeO]^{3+}$ species is reflected in a faster rate of hydroxylation relative to electron transfer and an increase in the production of 1-phenylethanol. The volume and flexibility of the amino acid are clearly important as shown by the fact that a phenylalanine residue is more effective at position T185 than

threonine, valine, or leucine. With T185F, the hydroxylation of ethylbenzene becomes the predominant reaction pathway, accounting for two-thirds of the flux through the third branch point. The effects of individual substitutions are approximately additive when combined in the triple mutant T101M–T185F–V247M. This suggests that there are no significant secondary effects on the protein structure as a result of combining the T101M, T185F, and V247M mutations and that these residues, despite their proximity, behave independently. Introducing T185F and V247M into the background of T101M reverses the effect of the initial substitution. T101M virtually eliminates ethylbenzene oxidation by denying substrate access to the heme. Steric bulk introduced in Tiers 2 and 3 forces the substrate toward the iron, perhaps causing the flexible methionine side chain to assume an alternate conformation, thus restoring hydroxylation activity. The steric repulsion between ethylbenzene and the two amino acid replacements in the upper tiers of the active site offsets the effect of the single substitution in the lower tier as shown by the larger fraction of 1-phenylethanol produced with the triple mutant relative to the wild-type enzyme. The positioning of ethylbenzene in the active site is primarily determined by the location and steric packing volume of the altered amino acid and also depends on the side chain's shape and flexibility. The results suggest that substrate access to the iron can be altered in a predictable fashion.

Molecular modeling of the mutations by rigid docking of ethylbenzene in the active site is consistent with the interpretations outlined above (Loida & Sligar, 1993). Molecular dynamics simulations should provide a more detailed description of structural determinants responsible for the partitioning of reducing equivalents at the oxidase branch point (Bass *et al.*, 1992a; Paulsen *et al.*, 1993). Publications prior to this paper, however, have not separated uncoupling due to branch point two from uncoupling at branch point three.

We have considered the possibility that repositioning ethylbenzene simply redistributes active-site water and that the changes in hydroxylation and oxidase activity are due to solvent processes. The interactions of ethylbenzene with P-450$_{cam}$ are not specific in nature as the active site has evolved discriminating specificity for a molecule with a radically different structure. Because the shape of the binding pocket in any of the mutant proteins is not complementary to the three-dimensional structure of ethylbenzene, the distribution of a small and penetrating water molecule would not be expected to correlate with the location of the amino acid substitutions introduced in the active site. Sequestered water can more readily adjust to changes in substrate orientation and amino acid side-chain conformations that are a result of thermal motions. While the diameter of a water molecule (2.8 Å) is roughly one-fifth that of the active site, the length and width of ethylbenzene are close to the dimensions of the binding pocket. Molecular dynamics simulations suggest that ethylbenzene is mobile in the active site, yet this molecule occupies a significant molecular volume; the general orientation of this substrate should be very responsive to alterations in the topology of the active site (Filipovic *et al.*, 1992; Fruetel *et al.*, 1992). Distribution of solvent is less affected by the shape of the cleft and is probably not responsible for the strong correlation between the position and size of the amino acid mutations and the oxidase activity. The changes in hydrogen peroxide liberation probably reflect the nonspecific response expected from alterations in water access to the iron.

The calculated volume changes upon substituting a single amino acid side chain are 30 Å^3 for Val to Ile or Met, 40 Å^3 for Thr to Leu, Ile, or Met, and 60 Å^3 for Thr to Phe. These correspond to a decrease of about 10, 15, and 25% in the size of the P-450$_{cam}$ binding site, respectively. The triple mutant closes the pocket by 50%. The extra bulk of the leucine, isoleucine, methionine, and phenylalanine side chains makes the active site more hydrophobic by filling volume otherwise occupied by water. The experimental results show that in all but one mutant, the hydrogen peroxide produced is less than with the wild-type protein and the largest decrease is observed for T101M–T185F–V247M (Figure 4A). The fact that the changes caused by the single mutations are additive indicates that the mechanism for altering the peroxide shunt in the enzyme is a first-order effect on the polarity or hydration of the active site and probably not a secondary perturbation of a related step in the cytochrome P-450 reaction (Wells, 1990). While the location, shape, and flexibility of the amino acid replacement are not factors in the partitioning of reducing equivalents at the second reaction cycle branch point, a rough correlation is observed with the steric packing volume of most of the mutations. This is taken as evidence that the key determinant controlling uncoupling at the level of the two-electron-reduced dioxygen-bound species is water distribution in the active site and solvent access to the iron. The increased polarity of the water-filled pocket would favor charge separation at the iron during the release of hydrogen peroxide anion. Additionally, active-site water could alter the putative hydrogen bond between T252 and peroxy-P-450$_{cam}$ intermediates, further destabilizing the complex. A role for water in these uncoupling processes may represent a universal feature of hemoprotein systems as it has previously been proposed for the autoxidation of myoglobin based on kinetic and thermodynamic studies of the wild-type protein and several active-site mutants (Carver *et al.*, 1992; Satoh & Shikama, 1981; Springer *et al.*, 1989).

The effect of the single mutation V247A on the autoxidation activity is not consistent with the interpretation presented above. There may be significant structural rearrangements with this particular mutant such that the active-site cleft is actually decreased in volume relative to wild-type. This interpretation is consistent with the lower dissociation constant observed with V247A and ethylbenzene. Another possibility is that the V247A substitution perturbs the proton-transfer pathway proposed recently (Gerber & Sligar, 1992). In P-450$_{cam}$, V247 is also close to other residues in the charge relay and hence may also perturb this hydrogen bond network.

Several lines of experimental evidence, including the kinetics of water binding to the iron and X-ray analysis of cytochrome P-450$_{cam}$ in the substrate-free and -bound forms, indicate that the access of water to the iron in the presence of a given substrate is correlated with the ferric spin-state equilibrium of the enzyme (Fisher & Sligar, 1987; Raag & Poulos, 1989). To the extent that the ferric spin equilibrium is a measure of solvent access to the heme, one might expect the peroxide liberation for this set of mutants to vary in accordance with the percentage of high-spin ferric heme iron. Our results show that no such relationship exists and suggest that water access as it is measured by the high-spin population is distinctly different from any role of water in the breakdown of reaction cycle intermediates.

The substrate binding equilibrium of cytochrome P-450$_{cam}$ is entropically driven at room temperature, presumably due to the release of ordered water around the free substrate and sequestered water from the active site (Griffin & Peterson,

1972). All of the mutant cytochrome P-450$_{cam}$ enzymes have decreased dissociation constants with ethylbenzene (Table II). The tighter binding of this substrate in the mutants is most likely due to the larger side chains of leucine, isoleucine, methionine, and phenylalanine which increase the hydrophobic interactions in the binary complex and allow a smaller fraction of solvent to remain in the binding pocket. There is no correlation between the changes in equilibrium binding energy and amino acid hydrophobicity as it is measured in partitioning experiments (Cornette *et al.*, 1987). This point is clearly exemplified by T185F and V247A which have dissociation constants of 80 and 60 μM, respectively. Clearly, the contributions of repulsive forces are difficult to estimate in this set of mutants, and the substrate binding equilibrium is not simply a function of the van der Waals volume of the mutated residue but is also dependent on the specific packing arrangement of nonpolar substituents in the active site. The added steric bulk in the mutant proteins could result in unfavorable steric hindrance between the mutated side chain and neighboring amino acids when camphor associates with the enzymes due to an overpacking of the active site. T185L is an interesting anomaly because it binds camphor 2-fold tighter than the wild-type protein. Presumably, the leucine side chain introduces no unfavorable steric contacts and makes hydrophobic interactions with the 10-carbon of camphor. For the wild-type enzyme, the specificity of binding camphor relative to ethylbenzene corresponds to a free energy difference of roughly -2.4 kcal mol^{-1}. The triple mutant should have a drastic effect on substrate binding because the total volume is reduced by half. Indeed, there is no preference for the native substrate camphor as the binding specificity is eliminated with this extensively reengineered protein. As in the case of hydrogen peroxide and water production, the changes in the dissociation constant with camphor and ethylbenzene caused by the individual mutations are additive.

The fact that the effects of the individual mutations are additive in the triple mutant and that in the substrate-free form the spectral features of the mutants are the same as wild-type would argue that specificity changes resulting from active-site mutations are not a result of large disruptions in the enzyme structure. X-ray crystallographic analysis of the proteins is necessary to confirm the absence of significant structural changes.

The present investigation shows that the flux through both the peroxide shunt and the oxidase pathway in P-450 is dependent on the structure of the substrate and is altered by active-site mutations. Recently, the "overall coupling" (Bass *et al.*, 1992a, Paulsen *et al.*, 1993) of NADH to hydroxylated product has been used as a probe to monitor the effect of specific protein–substrate interactions on the positioning of campor analogs in the P-450$_{cam}$ active site. The coupling of the reaction is an accurate probe for substrate recognition only if the partitioning of reducing equivalents at both the second and third branch points is determined. Analysis of the individual branch points is necessary to establish whether the changes in coupling are due to the peroxide shunt, as a result of active-site hydration, or the oxidase pathway, as a consequence of the substrate's position in the active site and proximity to the [FeO]$^{3+}$ intermediate. Theoretical analysis of coupling using molecular dynamics simulations is based on the time-dependent proximity and orientation of the substrate relative to the iron–oxo intermediate and therefore addresses only the third branch point of the reaction cycle (Bass *et al.*, 1992a; Filipovic *et al.*, 1992; Paulsen *et al.*, 1993).

Understanding the determinants for uncoupling is essential in attempts to redesign the P-450$_{cam}$ active site for new substrate specificities. The functional similarities between P-450 and many inorganic–organic catalysts commonly used in synthetic chemistry beg the issue of whether these strong oxidizing enzymes can be designed to perform novel chemical transformations not currently accessible (Allain *et al.*, 1993; Atkins & Sligar, 1989). As the reality of rational protein design draws near, the control of uncoupling reactions will be of the utmost importance in maximizing catalytic efficiency and reducing the output of destructive side products. The strategies for controlling reaction specificity outlined herein could also be useful in the design of biomimetic catalysts which are often limited by suicide inhibition, unproductive side reactions, and the release of partially reduced reaction intermediates.

In summary, we have attempted to develop a unified view for the role of substrate contact residues in P-450 catalysis. The catalytic steps leading up to the formation of the putative [FeO]$^{3+}$ intermediate are probably controlled by the protic amino acids of the distal pocket charge relay (Gerber & Sligar, 1992; Imai *et al.*, 1989; Martinis *et al.*, 1989). The side chains that form the internal surface of the active site are structurally distinct from the charge relay and do not directly participate in dioxygen chemistry, but through their role in determining substrate orientation and dynamics and active-site hydration, these residues have a dramatic effect on the fate of reaction cycle intermediates and the coupling of reducing equivalents to product. We have now shown that the partitioning between oxidase and hydroxylation activities at the iron–oxo species can be controlled to favor the production of either water or product alcohol by altering the topology of the active site. The access of ethylbenzene to the oxidizing species is the key determinant in tight coupling at the third reaction branch point and is rationally modulated by changing the position and steric packing volume of nonpolar amino acid substitutions in the binding pocket. The loss of reducing equivalents at the level of the reduced dioxygen-bound intermediate appears to be a function of active-site hydration. By adding steric bulk to the active site at a variety of different locations, the liberation of hydrogen peroxide is consistently decreased, and the effect is largest when the active-site hydrophobicity is maximized. The orientation of substrate in the buried binding pocket and active-site solvation of the heme iron represent general mechanisms of control of the reaction specificity at the oxidase pathway and autoxidation shunt for this superfamily of hemoproteins.

REFERENCES

Allain, E. J., Deng, L., Jacobson, E. N., & Hager, L. P. (1993) *J. Am. Chem. Soc. 115*, 4415–4416.

Atkins, W. M., & Sligar, S. G. (1987) *J. Am. Chem. Soc. 109*, 3754–3760.

Atkins, W. M., & Sligar, S. G. (1988a) *Biochemistry 27*, 1610–1616.

Atkins, W. M., & Sligar, S. G. (1988b) *J. Biol. Chem. 263*, 18842–18849.

Atkins, W. M., & Sligar, S. G. (1989) *J. Am. Chem. Soc. 111*, 2715–2717.

Bass, M. B., Filipovic, D., Sligar, S. G., & Ornstein, R. L. (1992a) *Protein Eng.* (submitted for publication).

Bass, M. B., Paulsen, M. D., & Ornstein, R. L. (1992b) *Proteins: Struct., Funct., Gent. 13*, 26–37.

Carver, T. E., Brontley, R. E., Singleton, E. W., Arduini, R. M., Quillin, M. L., Phillios, G. N., & Olson, J. S. (1992) *J. Biol. Chem. 267*, 14443–14450.

Collins, J. R., & Loew, G. H. (1988) *J. Biol. Chem. 263*, 3164–3170.
Cornette, J. L., Cease, K. B., Margalit, H., Spouge, J. L., Berzofsky, J. A., & Delisi, C. (1987) *J. Mol. Biol. 195*, 659–686.
Davies, M. D., Quin, L., Beck, J. L., Suslick, K. S., Koga, H., Horiuchi, T., & Sligar, S. G. (1990) *J. Am. Chem. Soc. 112*, 7396–7398.
DiPrimo, C., Hui Bon Hoa, G., Douzou, R., & Sligar, S. (1990) *Eur. J. Biochem. 193*, 383–386.
Estabrook, R. W., Hildebrandt, A. G., Baron, J., Netter, K. J., & Leibman, K. (1971) *Biochem. Biophys. Res. Commun. 42*, 132–135.
Filipovic, D., Paulsen, M. D., Loida, P. J., Sligar, S. G., & Ornstein, R. L. (1992) *Biochem. Biophys. Res. Commun. 189*, 488–495.
Fisher, M. T., & Sligar, S. G. (1985) *J. Am. Chem. Soc. 107*, 5018–5019.
Fisher, M. T., & Sligar, S. G. (1987) *Biochemistry 26*, 4797–4803.
Fruetel, J. A., Collins, J. R., Camper, D. L., Loew, G. H., & Ortiz de Montellano, P. R. (1992) *J. Am. Chem. Soc. 114*, 6987–6993.
Gelb, M. H., Heimbrook, D. C., Mälkönen, P., & Sligar, S. G. (1982) *Biochemistry 21*, 370–377.
Gelb, M. H., Mälkönen, P., & Sligar, S. (1982) *Biochem. Biophys. Res. Commun. 104*, 853–858.
Gerber, N. C., & Sligar, S. G. (1992) *J. Am. Chem. Soc. 114*, 8742.
Gorsky, L. D., Kopp, D. R., & Coon, M. J. (1984) *J. Biol. Chem. 259*, 6812–6817.
Gould, P., Gelb, M. H., & Sligar, S. G. (1981) *J. Biol. Chem. 256*, 6686–6691.
Griffin, B. W., & Peterson, J. A. (1972) *Biochemistry 11*, 4740–4746.
Groves, J. T., & McCluskey, G. A. (1976) *J. Am. Chem. Soc. 98*, 859–861.
Guengerich, F. P. (1991) *J. Biol. Chem. 266*, 10019–10022.
Gunsalus, I. C., & Wagner, G. C. (1978) *Methods Enzymol. 52*, 166–188.
Hui bon Hoa, G., & Marden, M. C. (1982) *Eur. J. Biochem. 124*, 311–315.
Imai, M., Shimada, H., Watanabe, Y., Matsushima-Hibiya, Y., Makino, R., Koga, H., Horiuchi, T., & Ishimura, Y. (1989) *Proc. Natl. Acad. Sci. U.S.A 86*, 7823–7827.
Ishimura, Y., Ullrich, V., & Peterson, J. A. (1971) *Biochem. Biophys. Res. Commun. 42*, 140–146.
Lipscomb, J. D., Sligar, S. G., Namtuedt, M. J., & Gunsalus, I. C. (1976) *J. Biol. Chem. 251*, 1116–1124.
Loida, P. J., & Sligar, S. G. (1993) *Protein Eng. 2*, 207–212.
Martinis, S. A. (1990) Ph.D. Thesis, University of Illinois, Urbana, IL.
Martinis, S. A., Atkins, W. M., Stayton, P. S., & Sligar, S. G. (1989) *J. Am. Chem. Soc. 111*, 9252–9253.
Paulsen, M. D., Bass, M. B., & Ornstein, R. L. (1991) *J. Biomol. Struct. Dyn. 9*, 187–203.
Paulsen, M. D., Filipovic, D., Sligar, S. G., & Ornstein, R. L. (1993) *Protein Sci. 2*, 357–365.
Poulos, T. L., Finzel, B. C., & Howard, A. J. (1987) *J. Mol. Biol. 195*, 687–700.
Raag, R., & Poulos, T. L. (1989) *Biochemistry 28*, 917–922.
Raag, R., & Poulos, T. L. (1991) *Biochemistry 30*, 2674–2684.
Richards, F. M. (1977) *Annu. Rev. Biophys. Bioeng. 6*, 151–175.
Satoh, Y., & Shikama, K. (1981) *J. Biol. Chem. 256*, 10272–10275.
Sligar, S. G. (1976) *Biochemistry 15*, 5399–5406.
Sligar, S. G., & Gunsalus, I. C. (1976) *Proc. Natl. Acad. Sci. U.S.A. 73*, 1078–1082.
Sligar, S. G., & Murray, R. I. (1986) in *Cytochrome P-450: Structure, Mechanism, and Biochemistry* (Ortiz de Montellano, P. R., Ed.) pp 429–503, Plenum Press, New York.
Sligar, S. G., Lipscomb, J. D., Debrunner, P. G., & Gunsalus, I. C. (1974) *Biochem. Biophys. Res. Commun. 61*, 290–296.
Springer, B. A., Egeberg, K. S., Sligar, S. G., Rohlfs, R. J., Mathews, A. J., & Olson, J. S. (1989) *J. Biol. Chem. 264*, 3057–3060.
Staudt, H., Lichtenberger, F., & Ullrich, V. (1974) *Eur. J. Biochem. 46*, 99–106.
Tyson, C. A., Lipscolm, J. D., & Gunsalus, I. C. (1972) *J. Biol. Chem. 247*, 5777–5784.
Walker, Griffin, B., & Peterson, J. A. (1972) *Biochemistry 11*, 4740–4746.
Weber, G. (1973) in *Molecular Biophysics* (Pullman, B., & Weisbluth, M., Eds.) pp 369–396, J. Wiley and Sons, New York.
Wells, J. A. (1990) *Biochemistry 29*, 8509–8517.
White, R. E., McCarthy, M. B., Egeberg, K. D., & Sligar, S. G. (1984) *Arch. Biochem. Biophys. 228*, 493–502.
Zhukov, A. A., & Archakov, A. I. (1982) *Biochem. Biophys. Res. Commun. 109*, 1982.